Using Polarized Spectroscopy to Investigate Order in Thin-Films of Ionic Self-Assembled Materials Based on Azo-Dyes

Miguel R. Carro-Temboury,* Martin Kühnel, Mariam Ahmad, Frederik Andersen, Ári Brend Bech, H. Krestian L. Bendixen, Patrick R. Nawrocki, Anders J. Bloch, Ilkay Bora, Tahreem A. Bukhari, Nicolai V. Bærentsen, Jens Carstensen, Smeeah Chima, Helene Colberg, Rasmus T. Dahm, Joshua A. Daniels, Nermin Dinckan, Mohamed El Idrissi, Ricci Erlandsen, Marc Førster, Yasmin Ghauri, Mikkel Gold, Andreas Hansen, Kenn Hansen, Mathias Helmsøe-Zinck, Mathias Henriksen, Sophus V. Hoffmann, Louise O. H. Hyllested, Casper Jensen, Amalie S. Kallenbach, Kirandip Kaur, Suheb R. Khan, Emil T. S. Kjær, Bjørn Kristiansen, Sylvester Langvad, Philip M. Lund, Chastine F. Munk, Theis Møller, Ola M. Z. Nehme, Mathilde Rove Nejrup, Louise Nexø, Simon Skødt Holm Nielsen, Nicolai Niemeier, Lasse V. Nikolajsen, Peter C. T. Nøhr, Dominik B. Orlowski, Marc Overgaard, Jacob Skaarup Ovesen, Lucas Paustian, Adam S. Pedersen, Mathias K. Petersen, Camilla M. Poulsen, Louis Praeger-Jahnsen, L. Sonia Qureshi, Nicolai Ree, Louise S. Schiermacher, Martin B. Simris, Gorm Smith, Heidi N. Smith, Alexander K. Sonne, Marko R. Zenulovic, Alma Winther Sørensen, Karina Sørensen, Emil Vogt, Andreas Væring, Jonas Westermann, Sevin B. Özcan and Thomas Just Sørensen *

Nano-Science Center & Department of Chemistry, University of Copenhagen, Universitetsparken 5, 2100 København Ø, Denmark; martin.kuhnel@nano.ku.dk (M.K.); mah@science.ku.dk (M.A.); zgb268@alumni.ku.dk (F.A.); dfb556@alumni.ku.dk (Á.B.B.); skf209@alumni.ku.dk (H.K.L.B.); tbu@science.ku.dk (P.R.N.); gcf945@alumni.ku.dk (A.J.B.); ilkay.bora@gmail.com (I.B.); xrs483@alumni.ku.dk (T.A.B.); gtw317@alumni.ku.dk (N.V.B.); cgm648@alumni.ku.dk (J.C.); mnb838@alumni.ku.dk (S.C.); wkj412@alumni.ku.dk (H.C.); lvf878@alumni.ku.dk (R.T.D.); tqn207@ku.dk (J.A.D.); jdq431@alumni.ku.dk (N.D.); lnk170@alumni.ku.dk (M.E.I.); dgk483@alumni.ku.dk (R.E.); dhm812@alumni.ku.dk (M.F.); wqn556@alumni.ku.dk (Y.G.); fbm685@alumni.ku.dk (M.G.); wjg795@alumni.ku.dk (A.H.); rjf884@alumni.ku.dk (K.H.); bpg317@alumni.ku.dk (M.H.-Z.); tqn207@alumni.ku.dk (M.H.); vxk757@alumni.ku.dk (S.V.H.); rsz113@alumni.ku.dk (L.O.H.H.); pxv130@alumni.ku.dk (C.J.); smh645@alumni.ku.dk (A.S.K.); nhs827@alumni.ku.dk (K.K.); qwm886@alumni.ku.dk (S.R.K.); sgz864@alumni.ku.dk (E.T.S.K.); vtz390@alumni.ku.dk (B.K.); cts952@alumni.ku.dk (S.L.); sqv821@alumni.ku.dk (P.M.L.); chastine.munk@ind.ku.dk (C.F.M.); jzg995@alumni.ku.dk (T.M.); dtw667@alumni.ku.dk (O.M.Z.N.); bnw543@alumni.ku.dk (M.R.N.); gtf274@alumni.ku.dk (L.N.); djq495@alumni.ku.dk (S.S.H.N.); zvl379@alumni.ku.dk (N.N.); fwn674@alumni.ku.dk (L.V.N.); hgv633@alumni.ku.dk (P.C.T.N.); mnc612@alumni.ku.dk (D.B.O.); marc.overgaard@nano.ku.dk (M.O.); kvn491@alumni.ku.dk (J.S.O.); cfh645@alumni.ku.dk (L.P.); zwx958@alumni.ku.dk (A.S.P.); scd880@alumni.ku.dk (M.K.P.); bcr102@alumni.ku.dk (C.M.P.); bvh517@alumni.ku.dk (L.P.-J.); ptr511@alumni.ku.dk (L.S.Q.); cmh133@alumni.ku.dk (N.R.); nwr275@alumni.ku.dk (L.S.S.); dsk326@ku.dk (M.B.S.); dsk326@alumni.ku.dk (G.S.); cfh645@alumni.ku.dk (H.N.S.); zwx958@alumni.ku.dk (A.K.S.); markozenulovic@gmail.com (M.R.Z.); alma.soerensen@sund.ku.dk (A.W.S.); marc.overgaard@chem.ku.dk (K.S.); bvh517@ku.dk (E.V.); qwm886@ku.dk (A.V.); jdq431@ku.dk (J.W.); sgz864@ku.dk (S.B.Ö.)

* Correspondence: miguel@chem.ku.dk (M.R.C.-T.); tjs@chem.ku.dk (T.J.S.); Tel.: +45-3532-0213 (T.J.S.)

nanomaterials

Table of contents

Author Contributions

Miguel R. Carro-Temboury designed the polarized optical experiments and the data analysis template, validated data analysis, and assisted in the writing of the paper.

Martin Kühnel recorded and helped analyzing the AFM micrographs, validated data analysis, and assisted in the writing of the paper.

Mariam Ahmad, Frederik Andersen, Ári B. Bech, H. Krestian L. Bendixen, Patrick R. N. Blichfeldt, Anders J.Bloch, Tahreem A. Bukhari, Nicolai V.Bærentsen, Jens Carstensen, Smeeah Chima, Helene Colberg, Rasmus T. Dahm, Joshua A.Daniels, Nermin Dinckan, Mohamed El Idrissi, Ricci F.Erlandsen, Marc Førster, Yasmin Ghauri, Mikkel Gold, Andreas Hansen, Kenn Hansen, Mathias Helmsøe-Zinck, Mathias Henriksen, Sophus V. Hoffmann, Louise O. H. Hyllested, Casper Jensen, Amalie S. Kallenbach, Kirandip Kaur, Suheb R. Khan, Emil T. S. Kjær, Bjørn Kristiansen, Sylvester H. Langvad, Philip M. Lund, Chastine F. Munk, Theis Møller, Ola M. Z. Nehme, Mathilde R. Nejrup, Louise Nexø, Simon Skødt Holm Nielsen, Nicolai Niemeier, Lasse V. Nikolajsen, Peter C. T. Nøhr, Dominik B. Orlowski, Jacob S. Ovesen, Lucas Paustian, Adam S. Pedersen, Mathias K. Petersen, Camilla M. Poulsen, Louis Praeger-Jahnsen, L. Sonia Qureshi, Nicolai Ree, Louise S. Schiermacher, Martin B. Simris, Gorm Smith, Heidi N. Smith, Alexander K. Sonne, Marko R. Zenulovic, Alma L. W. Sørensen, Karina Sørensen, Emil Vogt, Andreas Væring, Jonas Westermann, Sevin B. Özcan, designed the experiment, synthesized, purified and characterized the investigated materials. Prepared thin films, XRD powder samples and investigated the former using optical microscopy and AFM. Analysed the composition of the compounds, analyzed the data from polarized spectroscopy and interpreted the structure related data. Read and commented on/corrected the final manuscript.

Ilkay Bora supervised the synthesis and characterisation of the materials, validated elemental analysis and mass spectrometry data, and read and commented on the final draft of the manuscript.

Marc H. Overgaard helped/recorded optical microscopy images. Read and commented on the final manuscript.

Thomas Just Sørensen designed the experiments, helped in the synthesis and data analysis. Compiled the supporting information and wrote the paper.

Data Analysis

Scripts for the programs used for data analysis are supplied as part of the supporting information. Three scripts are supplied.

- Nano1_StretchedPolymers.m
- Nano1_ThinFilmAngles.m
- Nano1_OrientationTriangle.m

The data is loaded as x: wavelength in nm; y: absorbance from e.g. CSV files in the first two programs in order to determine ϕ_{fz} and α_{fz} (see main text).

The last program plots the orientation triangles used in the main text Figure 4b and Figure S84–85.

Allura red BZK10 Hold 14

Optical Microscopy
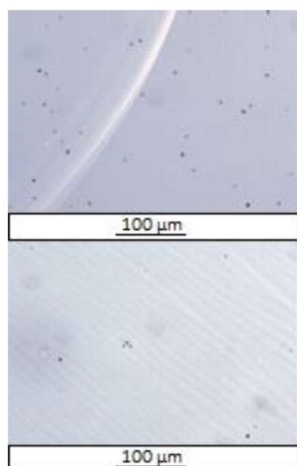
Figure S1. Wide field optical microscopy images of the edge (top) and a central region (bottom) of a thin film.

Atomic Force Microscopy
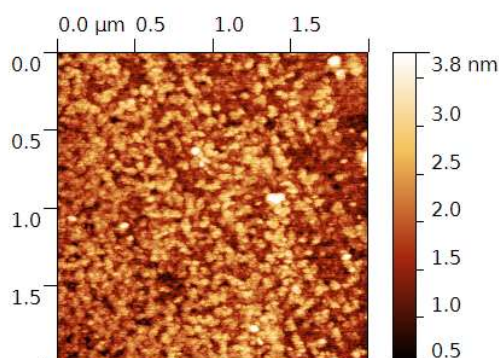
Figure S2. Atomic force microscopy (AFM) micrograph of the central region of a thin film. Distances determined from AFM; No distinct heights found.

Polarised Spectroscopy

| (A) | (B) | (C) |
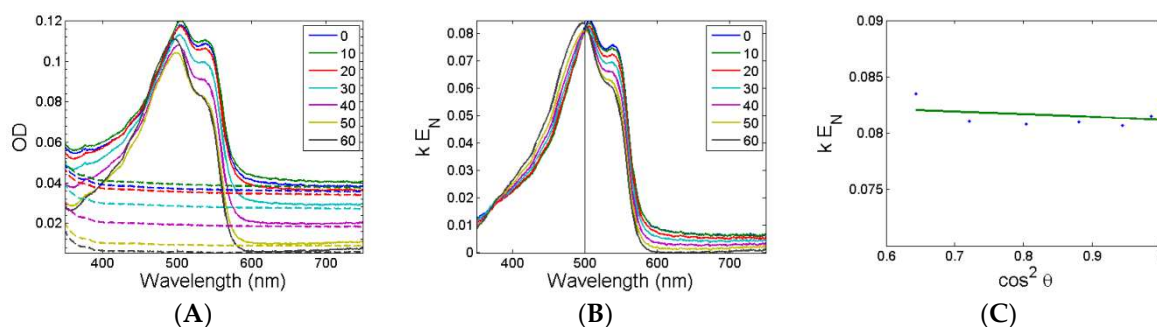
Figure S3. (**A**) Raw data from polarized optical spectroscopy (tilt angles from 0° to 60° in steps of 10). The spin coated films are represented with solid lines and the background from the glass with dashed lines. (**B**) Corrected spectra given by the constant k times the absorption coefficient E_N. (**C**) Linear regression at the maximum of the emission to find α_{fZ}.

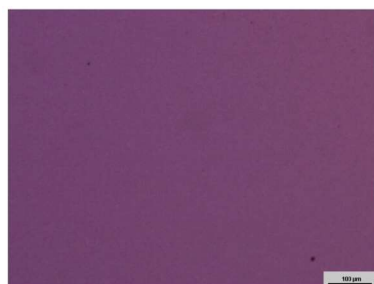**Allura red BZK12 Hold 15**

Optical Microscopy
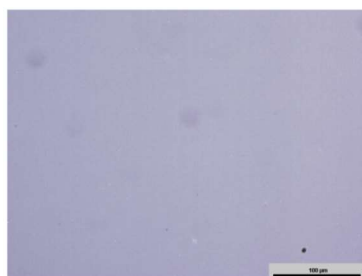
Figure S4. Wide field optical microscopy image of the central region of a thin film.
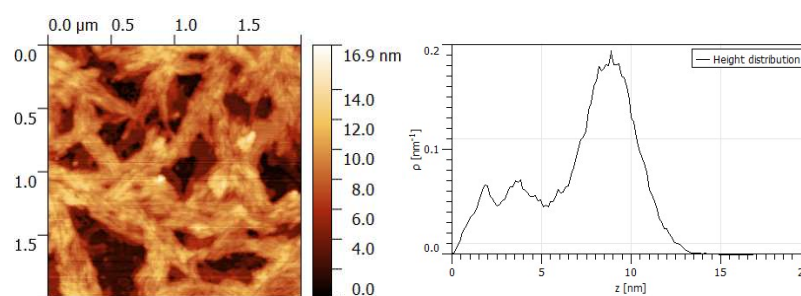
Atomic Force Microscopy
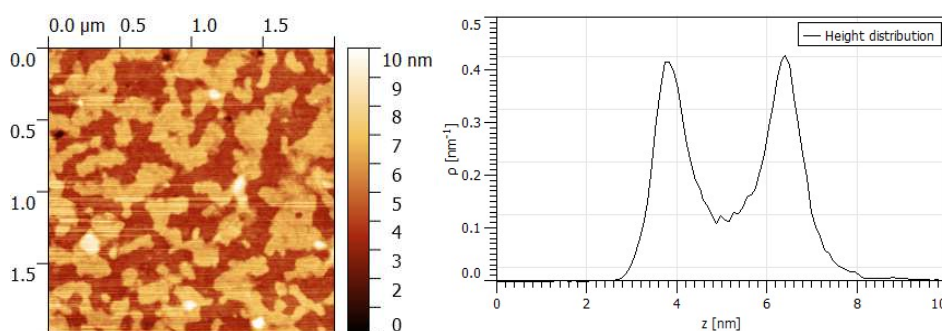
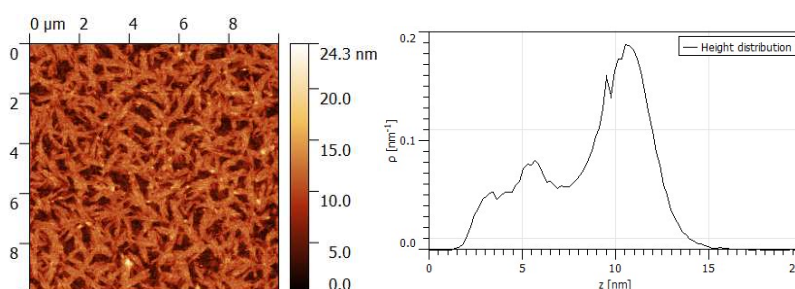**Figure S5.** AFM micrograph and height distribution (entire image) from the central region of a thin film.
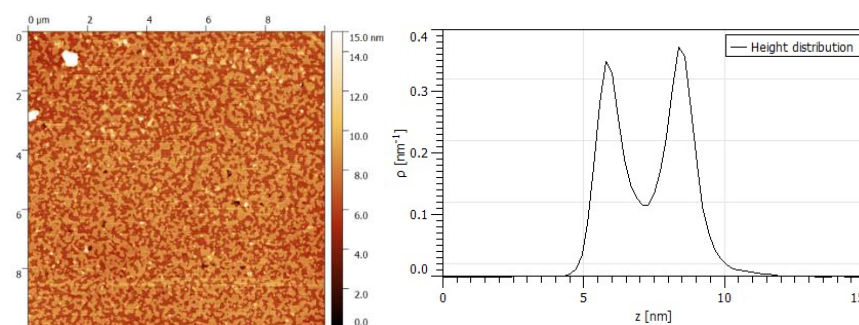
Figure S6. AFM micrograph and height distribution (entire image) from the central region of a thin film.
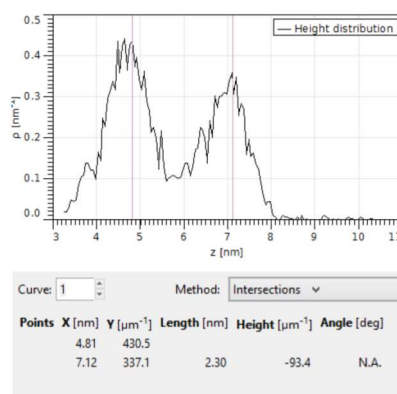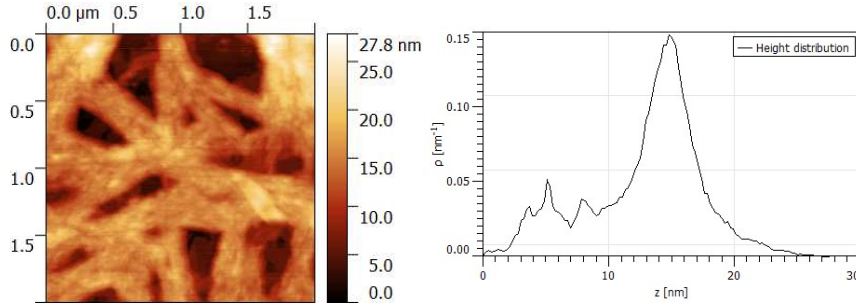

Figure S7. Height distribution taken from a local area in the image given in Figure S6.
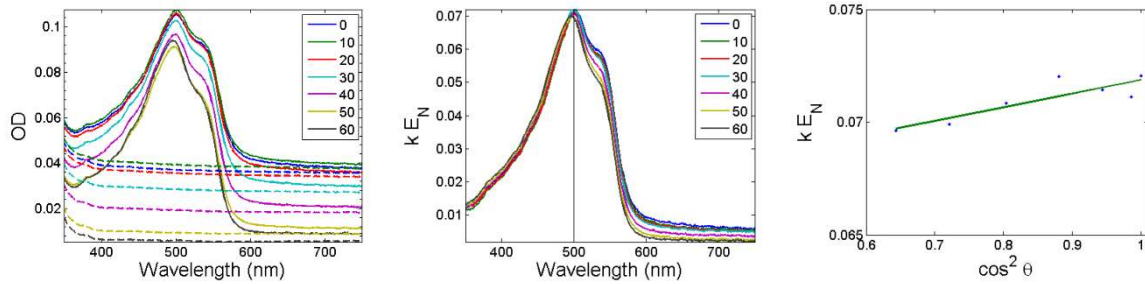
Polarized Spectroscopy
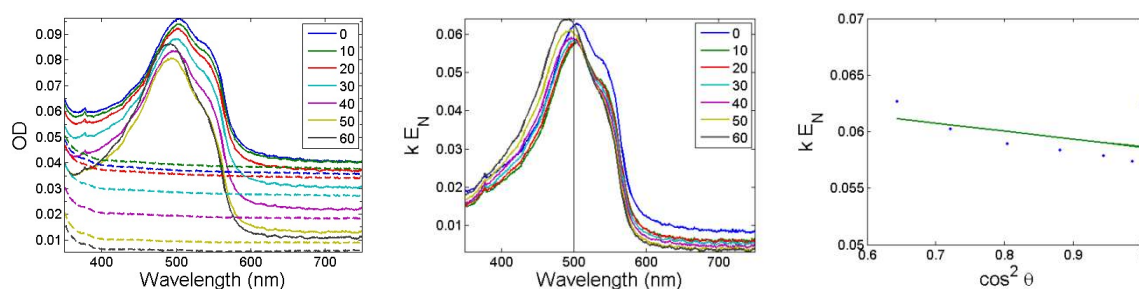
Figure S8. (**Left**) Raw data from polarized optical spectroscopy (tilt angles from 0° to 60° in steps of 10). The spin coated films are represented with solid lines and the background from the glass with dashed lines. (**Center**) Corrected spectra given by the constant k times the absorption coefficient E_N. (**Right**) Linear regression at the maximum of the emission to find α_{fZ}.

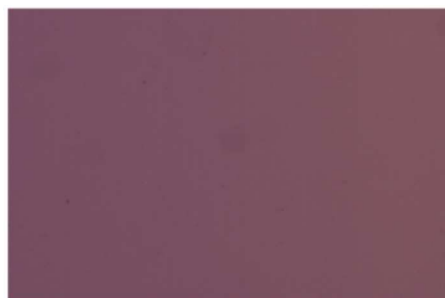**Allura red BZK14 Hold 9**

Optical Microscopy

Figure S9. Wide field optical microscopy image of the central region of a thin film.
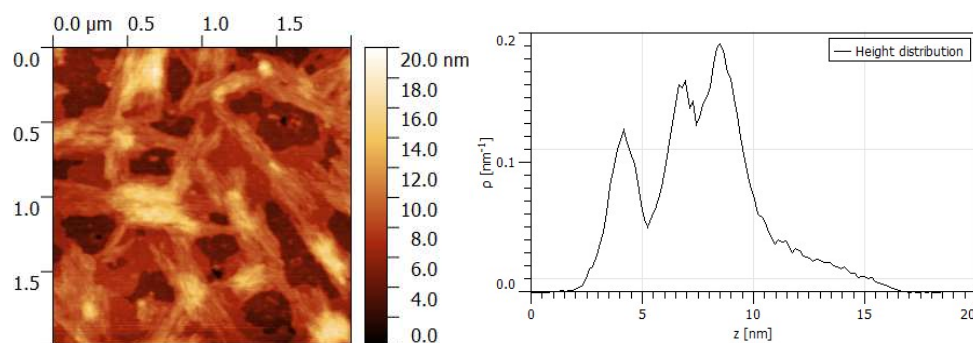
Atomic Force Microscopy

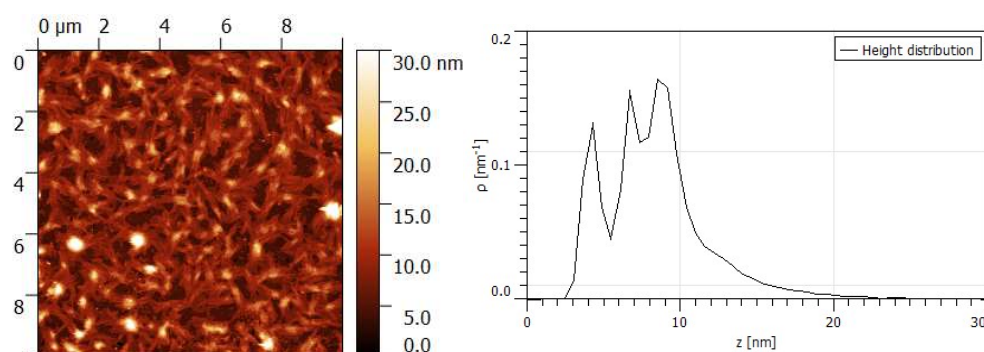**Figure S10.** AFM micrograph and height distribution (entire image) from the central region of a thin film.

Figure S11. AFM micrograph and height distribution (entire image) from the central region of a thin film.

Figure S12. AFM micrograph and height distribution (entire image) from the central region of a thin film.
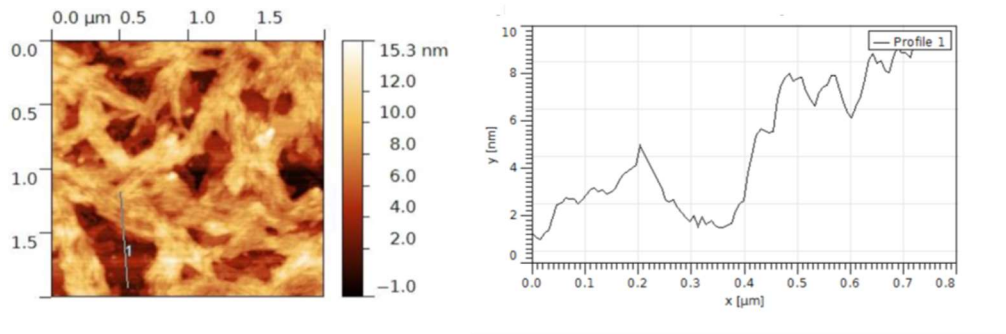
Figure S13. AFM micrograph and height profile (see line in image) from the central region of a thin film.

Polarized Spectroscopy

Figure S14. (**Left**) Raw data from polarized optical spectroscopy (tilt angles from 0° to 60° in steps of 10). The spin coated films are represented with solid lines and the background from the glass with dashed lines. (**Center**) Corrected spectra given by the constant k times the absorption coefficient E_N. (**Right**) Linear regression at the maximum of the emission to find α_{fZ}.

Allura red BZK16 Hold 4

Optical Microscopy

Figure S15. Wide field optical microscopy image of the central region of a thin film

Atomic Force Microscopy.

Figure S16. AFM micrograph and height distribution (entire image) from the central region of a thin film.

Figure S17. AFM micrograph and height distribution (entire image) from the central region of a thin film.
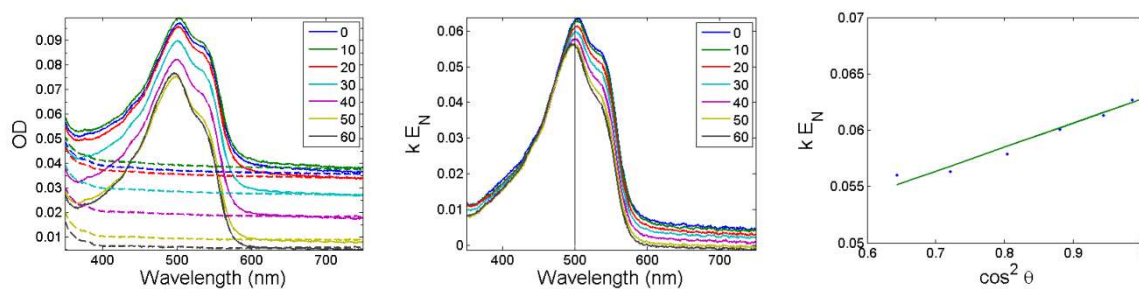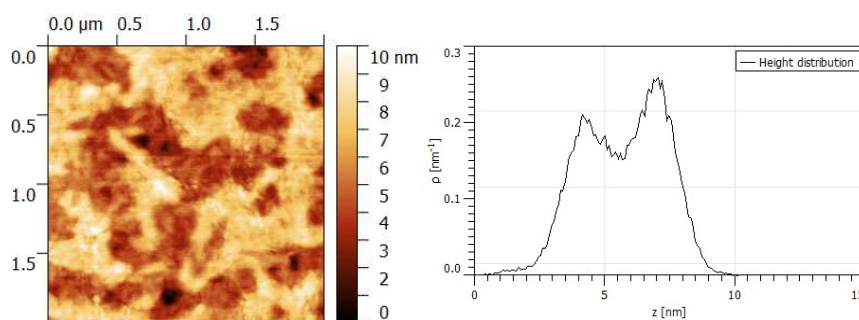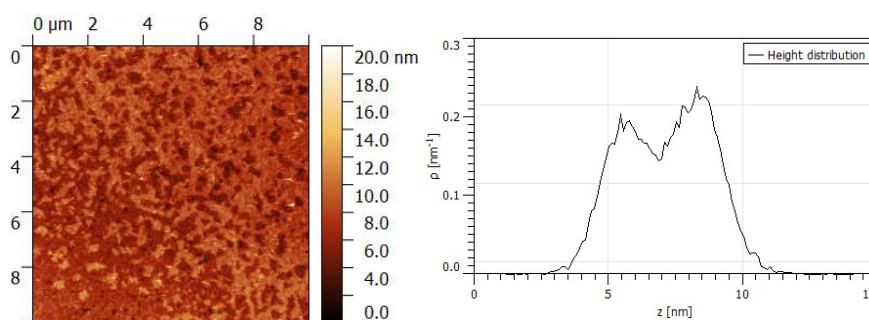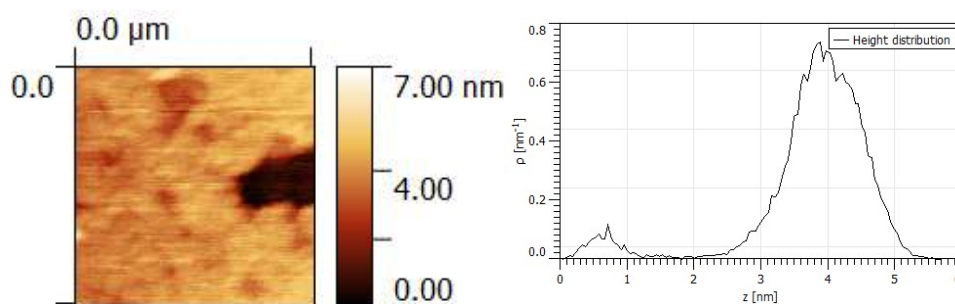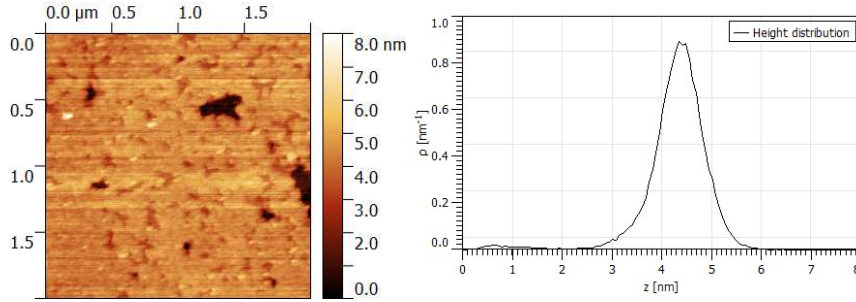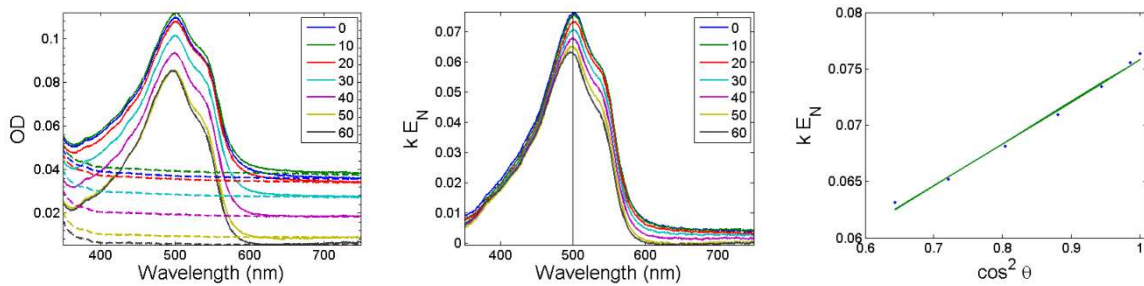
Polarized Spectroscopy

Figure S18. (**Left**) Raw data from polarized optical spectroscopy (tilt angles from 0° to 60° in steps of 10). The spin coated films are represented with solid lines and the background from the glass with dashed lines. (**Center**) Corrected spectra given by the constant k times the absorption coefficient E_N. (**Right**) Linear regression at the maximum of the emission to find α_{fZ}.

Allura red BZK18 Hold 10

Optical Microscopy
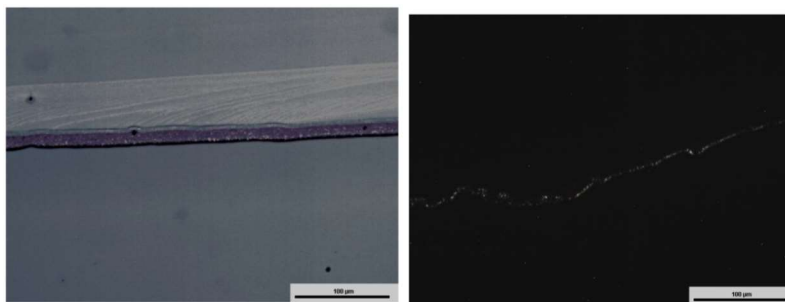
Figure S19. Wide field optical microscopy (top) and dark field microscopy (bottom) images of the edge of a thin film.

Atomic Force Microscopy

Figure S20. AFM micrograph and height distribution (entire image) from the central region of a thin film.

Figure S21. AFM micrograph and height distribution (entire image) from the central region of a thin film.
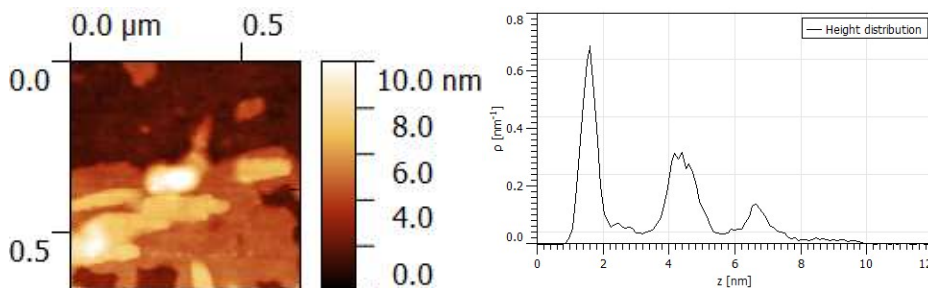

Figure S22. AFM micrograph and height distribution (entire image) from the central region of a thin film.

Figure S23. AFM micrograph and height distribution (entire image) from the central region of a thin film.

Polarized Spectroscopy

Figure S24. Left) Raw data from polarized optical spectroscopy (tilt angles from 0° to 60° in steps of 10). The spin coated films are represented with solid lines and the background from the glass with dashed lines. Center) Corrected spectra given by the constant k times the absorption coefficient E_N. Right) Linear regression at the maximum of the emission to find α_{fz}.

Bordeaux red BZK10 Hold 12

Optical Microscopy

Figure S25. Wide field optical microscopy image of the edge of a thin film.

Atomic Force Microscopy

Figure S26. AFM micrograph and height distribution (entire image) from the central region of a thin film.
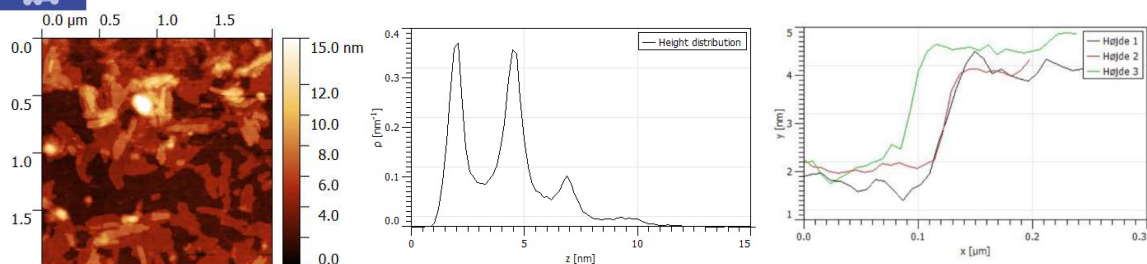
Figure S27. AFM micrograph and height distribution (entire image), and height profiles from the central region of a thin film.
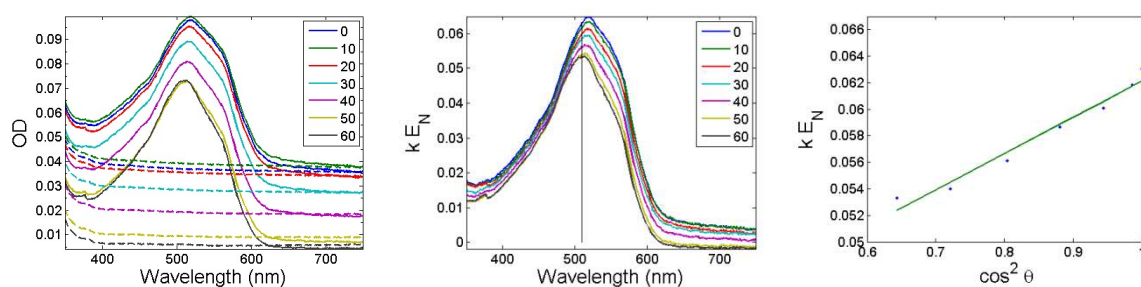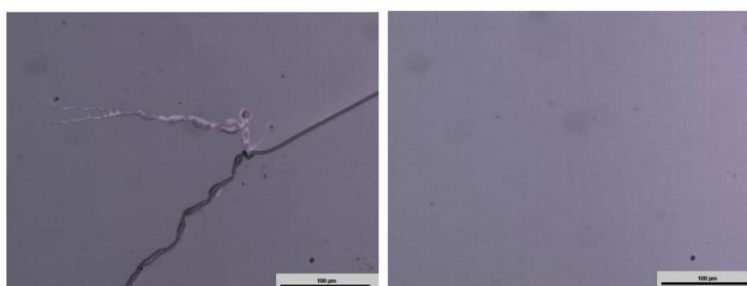
Polarized Spectroscopy

Figure S28. Left) Raw data from polarized optical spectroscopy (tilt angles from 0° to 60° in steps of 10). The spin coated films are represented with solid lines and the background from the glass with dashed lines. Center) Corrected spectra given by the constant k times the absorption coefficient E_N. Right) Linear regression at the maximum of the emission to find α_{fZ}.

Bordeaux red BZK12 Hold 13

Optical Microscopy

Figure S29. Wide field optical microscopy images of the edge (top) and central region (bottom) of a thin film.
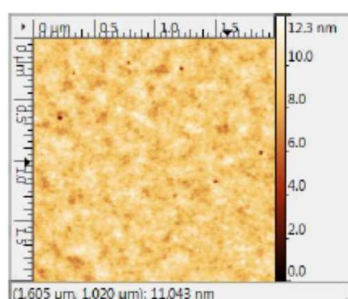
Atomic Force Microscopy

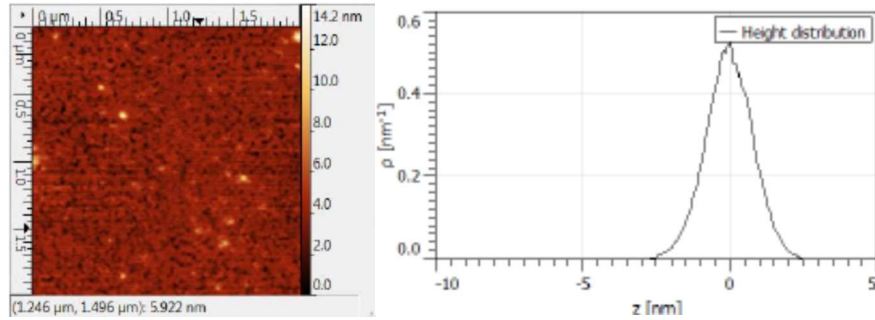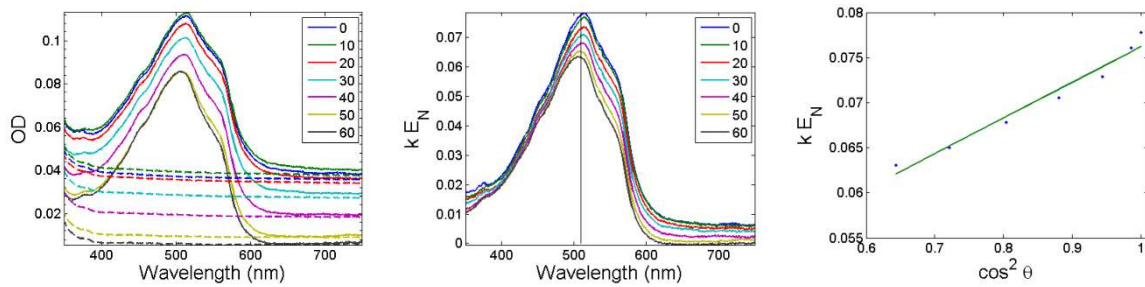**Figure S30.** AFM micrograph from the central region of a thin film.

Figure S31. AFM micrograph and height distribution (entire image) from the central region of a thin film.

Polarized Spectroscopy

Figure S32. Left) Raw data from polarized optical spectroscopy (tilt angles from 0° to 60° in steps of 10). The spin coated films are represented with solid lines and the background from the glass with dashed lines. Center) Corrected spectra given by the constant k times the absorption coefficient E_N. Right) Linear regression at the maximum of the emission to find α_{fz}.

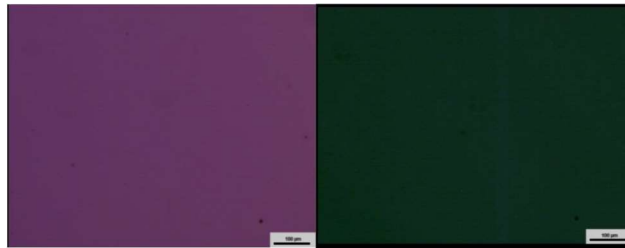**Bordeaux red BZK14 Hold 8**

Optical Microscopy

Figure S33. Wide field optical microscopy (top) and dark field microscopy (bottom) images of the edge of a thin film.
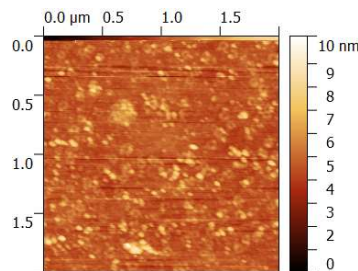
Atomic Force Microscopy

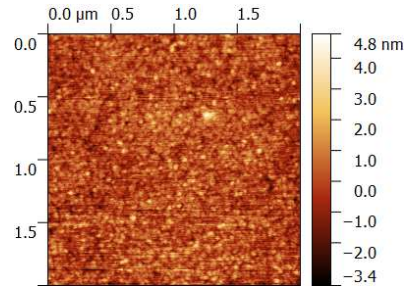**Figure S34.** AFM micrograph from the central region of a thin film.

Figure S35. AFM micrograph from the central region of a thin film.
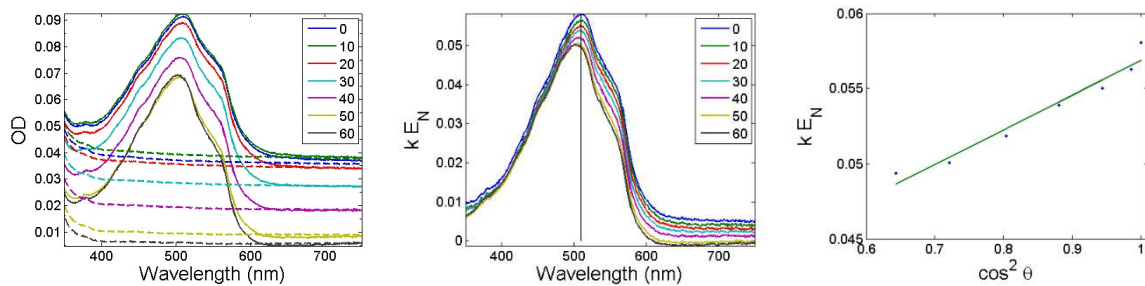
Polarized Spectroscopy

Figure S36. Left) Raw data from polarized optical spectroscopy (tilt angles from 0° to 60° in steps of 10). The spin coated films are represented with solid lines and the background from the glass with dashed lines. Center) Corrected spectra given by the constant k times the absorption coefficient E_N. Right) Linear regression at the maximum of the emission to find α_{fZ}.

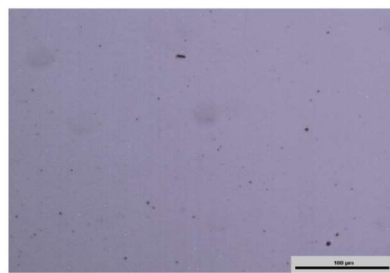**Bordeaux red BZK16 Hold 11**

Optical Microscopy

Figure S37. Wide field optical microscopy image of the central region of a thin film.
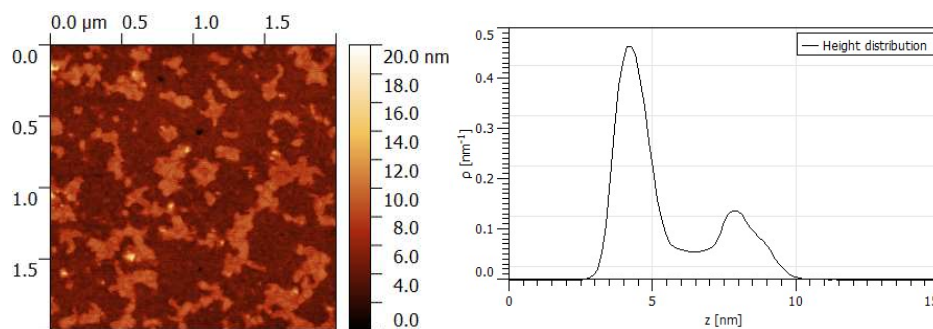
Atomic Force Microscopy

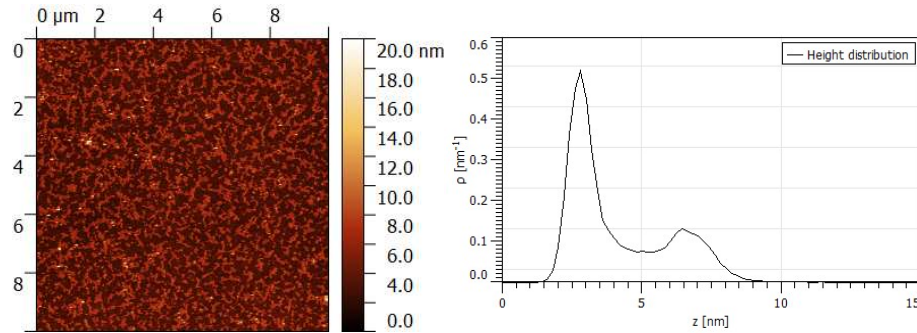**Figure S38.** AFM micrograph and height distribution (entire image) from the central region of a thin film.

Figure S39. AFM micrograph and height distribution (entire image) from the central region of a thin film.
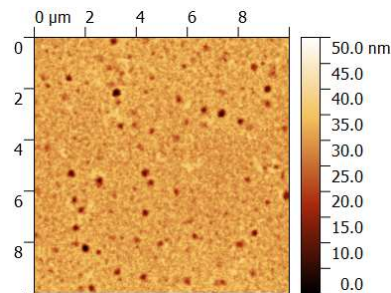

Figure S40. AFM micrograph from the central region of a thin film.
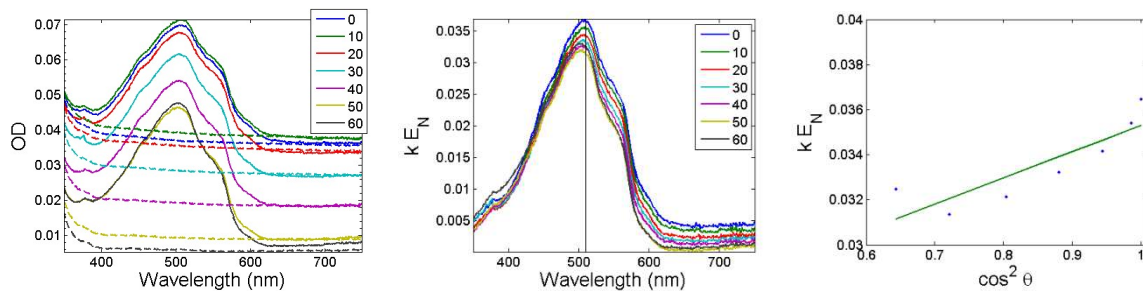
Polarized Spectroscopy

Figure S41. Left) Raw data from polarized optical spectroscopy (tilt angles from 0° to 60° in steps of 10). The spin coated films are represented with solid lines and the background from the glass with dashed lines. Center) Corrected spectra given by the constant k times the absorption coefficient E_N. Right) Linear regression at the maximum of the emission to find α_{fZ}.

Bordeaux red BZK18 Hold 16
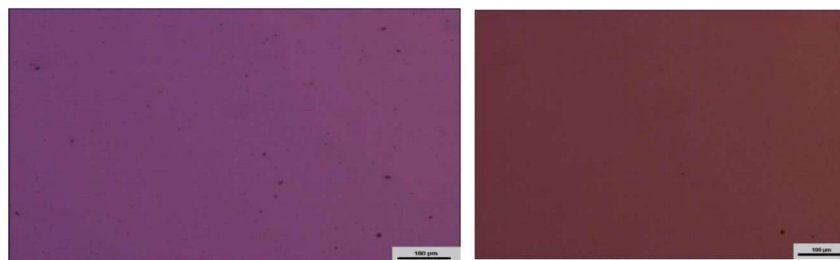
Optical Microscopy

Figure S42. Wide field optical microscopy (top) and dark field microscopy (bottom) images of the edge of a thin film.
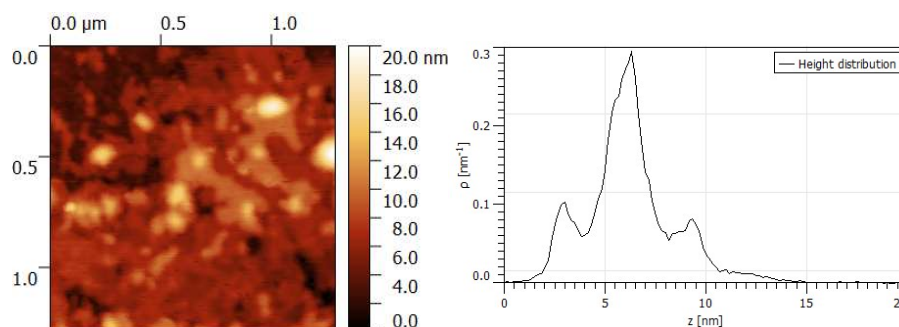
Atomic Force Microscopy

Figure S43. AFM micrograph and height distribution (entire image) from the edge of a thin film.
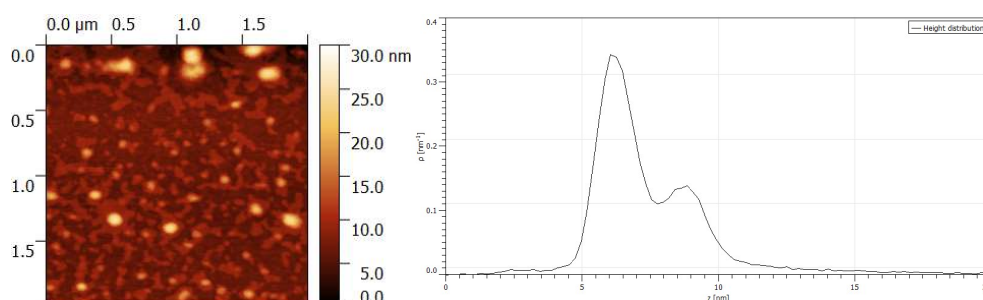

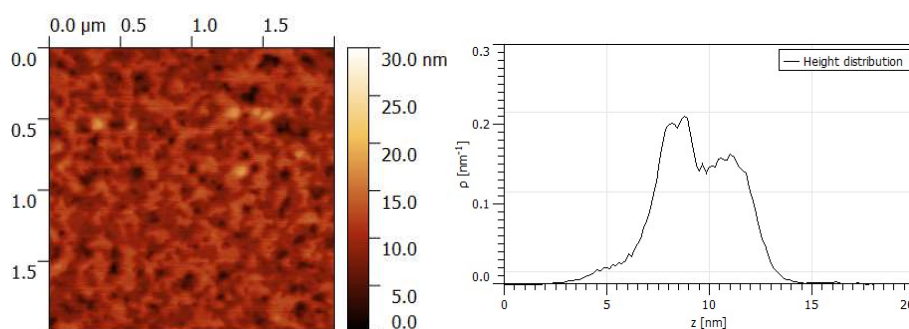**Figure S44.** AFM micrograph and height distribution (entire image) from the edge of a thin film.

Figure S45. AFM micrograph and height distribution (entire image) from the central region of a thin film.
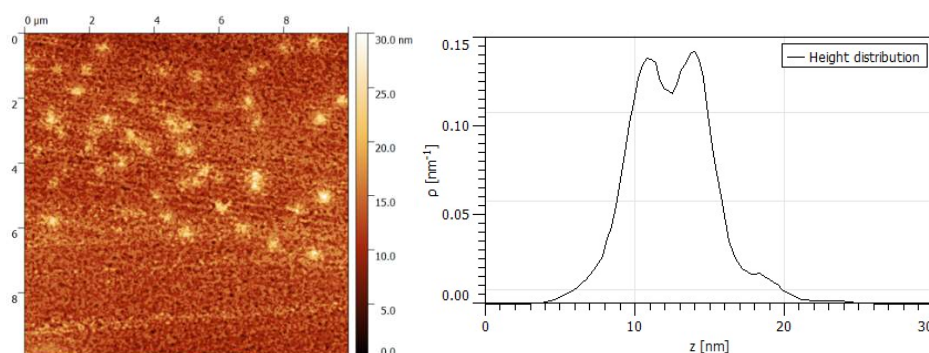

Figure S46. AFM micrograph and height distribution (entire image) from the central region of a thin film.
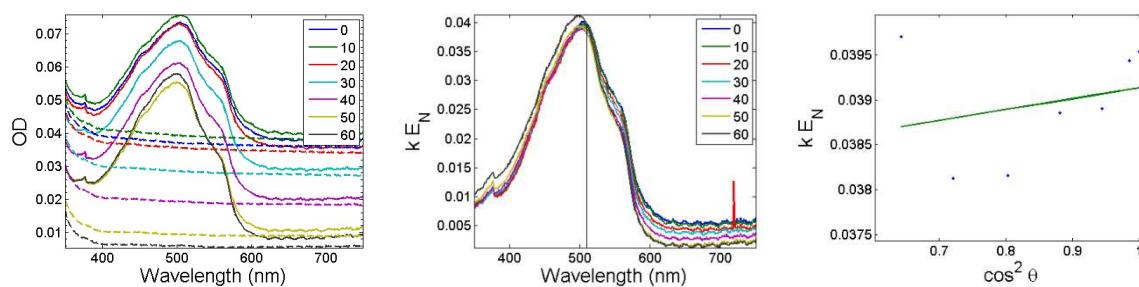
Polarized Spectroscopy

Figure S47. (**Left**) Raw data from polarized optical spectroscopy (tilt angles from 0° to 60° in steps of 10). The spin coated films are represented with solid lines and the background from the glass with dashed lines. (**Center**) Corrected spectra given by the constant k times the absorption coefficient E_N. (**Right**) Linear regression at the maximum of the emission to find α_{fZ}.

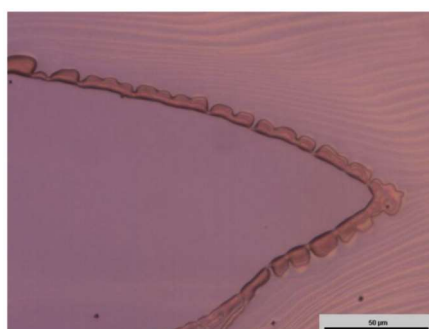## Amaranth BZK10 Hold 3

Optical Microscopy

Figure S48. Wide field optical microscopy image of the edge of a thin film.
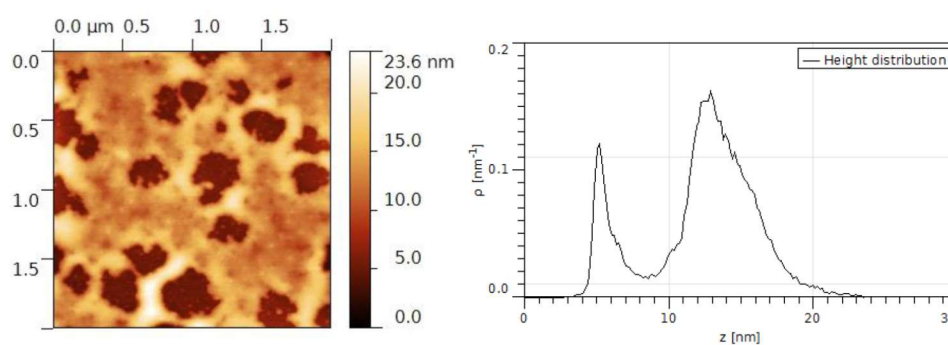
Atomic Force Microscopy

Figure S49. AFM micrograph and height distribution (entire image) from the central region of a thin film.
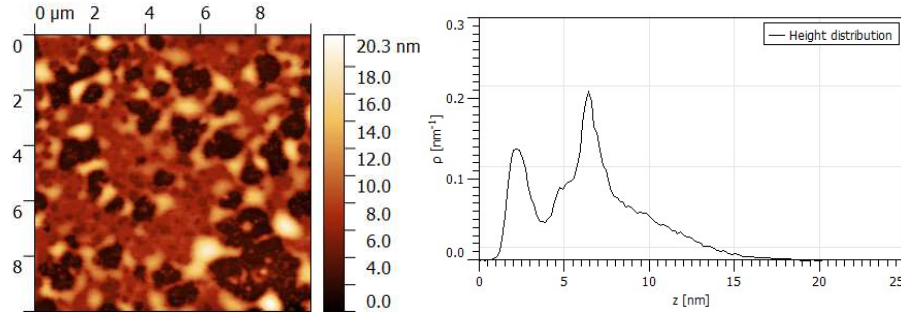
Figure S50. AFM micrograph and height distribution (entire image) from the central region of a thin film.

Figure S51 AFM micrograph and height distribution (entire image) from the central region of a thin film.

Figure S52. AFM micrograph and height distribution (entire image) from the central region of a thin film.
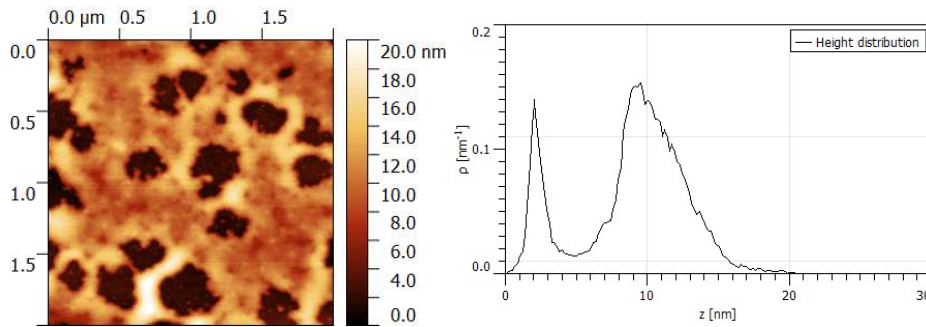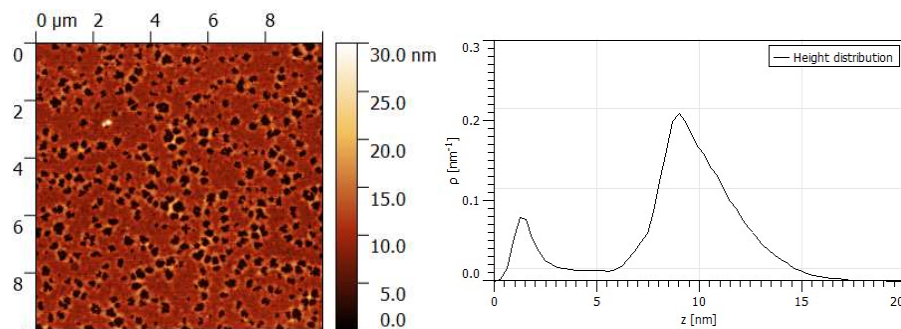
Polarized Spectroscopy

Figure S53. Left) Raw data from polarized optical spectroscopy (tilt angles from 0° to 60° in steps of 10). The spin coated films are represented with solid lines and the background from the glass with dashed lines. Center) Corrected spectra given by the constant k times the absorption coefficient E_N. Right) Linear regression at the maximum of the emission to find α_{fz}.

Amaranth BZK12 Hold 1

Optical Microscopy

Figure S54. Wide field optical microscopy image of the central region of a thin film.

Atomic Force Microscopy

Figure S55. AFM micrograph from the central region of a thin film.

Figure S56. AFM micrograph from the central region of a thin film.
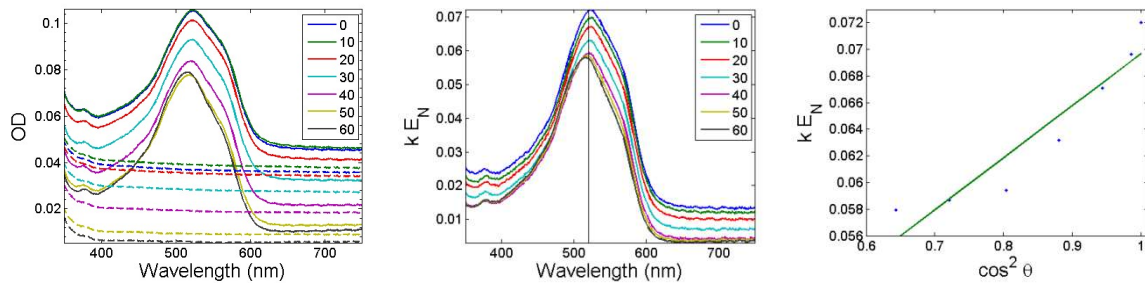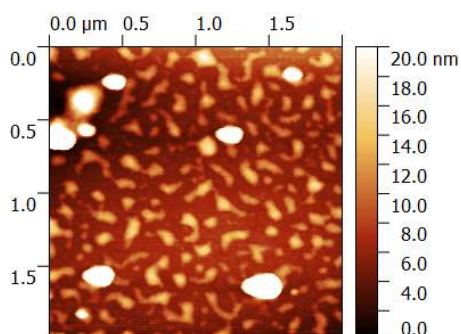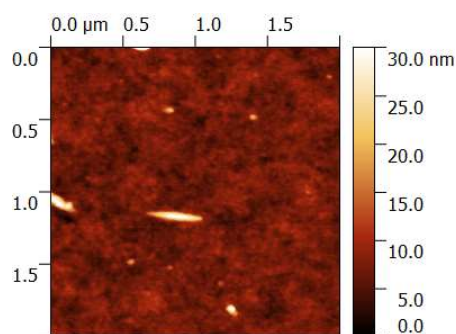
Polarized Spectroscopy

Figure S57. Left) Raw data from polarized optical spectroscopy (tilt angles from 0° to 60° in steps of 10). The spin coated films are represented with solid lines and the background from the glass with

dashed lines. Center) Corrected spectra given by the constant k times the absorption coefficient E_N. Right) Linear regression at the maximum of the emission to find α_{fZ}.

Amaranth BZK14 Hold 6

Optical Microscopy

Figure S58. Wide field optical microscopy image of the edge of a thin film.

Atomic Force Microscopy
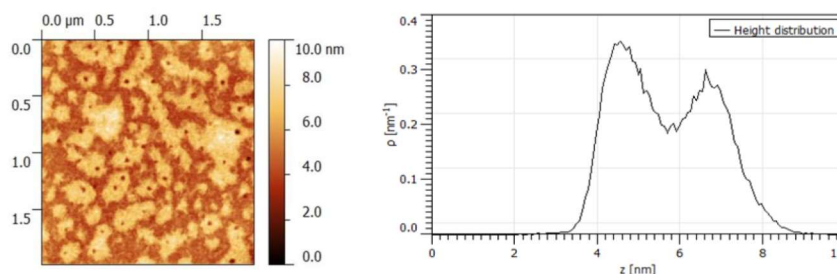
Figure S59. AFM micrograph and height distribution (entire image) from the central region of a thin film.
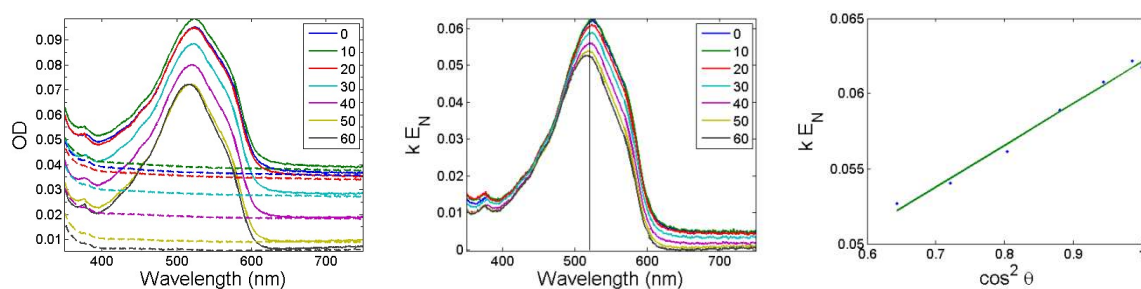
Polarized Spectroscopy

Figure S60. Left) Raw data from polarized optical spectroscopy (tilt angles from 0° to 60° in steps of 10). The spin coated films are represented with solid lines and the background from the glass with dashed lines. Center) Corrected spectra given by the constant k times the absorption coefficient E_N. Right) Linear regression at the maximum of the emission to find α_{fZ}.

Amaranth BZK16 Hold 5

Optical Microscopy

Figure S61. Wide field optical microscopy images of the edge (top) and central region (bottom) of a thin film.

Atomic Force Microscopy
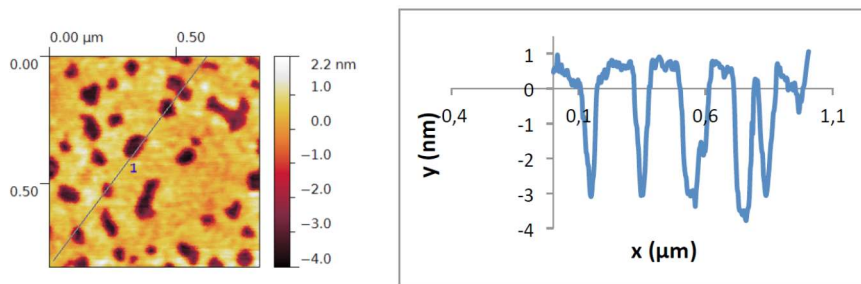
Figure S62. AFM micrograph and height profile (see line in image) from the central region of a thin film.
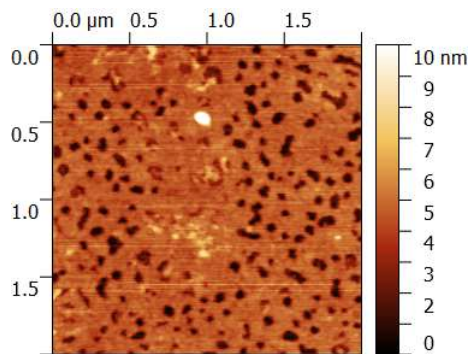
Figure S63. AFM micrograph from the central region of a thin film.
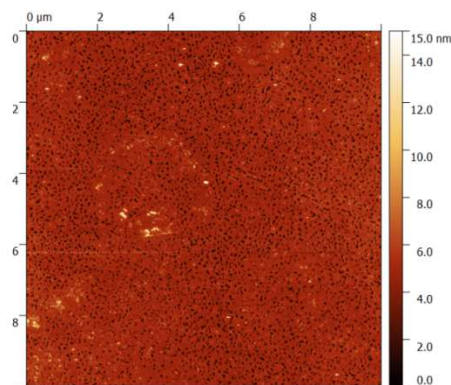
Figure S64. AFM micrograph from the central region of a thin film.

Figure S65. AFM micrograph and height profile from the central region of a thin film.

Figure S66. AFM micrograph from the edge of a thin film. Polarized Spectroscopy.
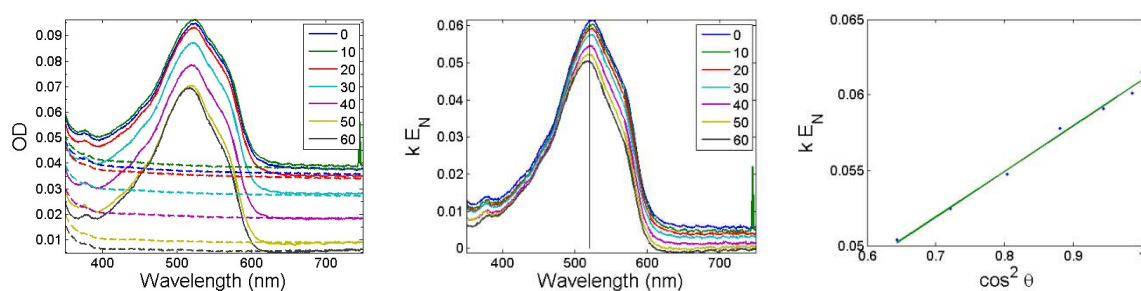
Polarized Spectroscopy

Figure S67. Left) Raw data from polarized optical spectroscopy (tilt angles from 0° to 60° in steps of 10). The spin coated films are represented with solid lines and the background from the glass with dashed lines. Center) Corrected spectra given by the constant k times the absorption coefficient E_N. Right) Linear regression at the maximum of the emission to find α_{fZ}.

Amaranth BZK18 Hold 2
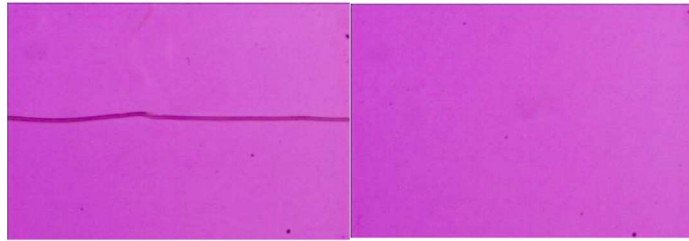
Optical Microscopy

Figure S68. Wide field optical microscopy images of the edge (top) and central region (bottom) of a thin film.

Atomic Force Microscopy

Figure S69. AFM micrograph and height distribution (part of image) from the central region of a thin film.
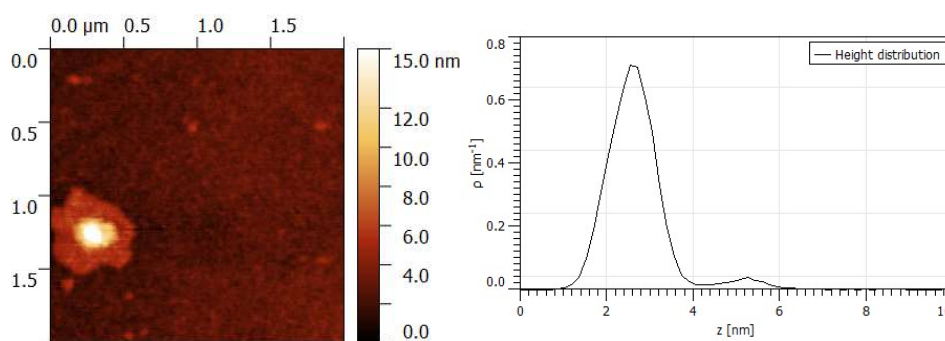
Figure S70. AFM micrograph and height distribution (entire image) from the central region of a thin film.

Figure S71. AFM micrograph from the central region of a thin film.

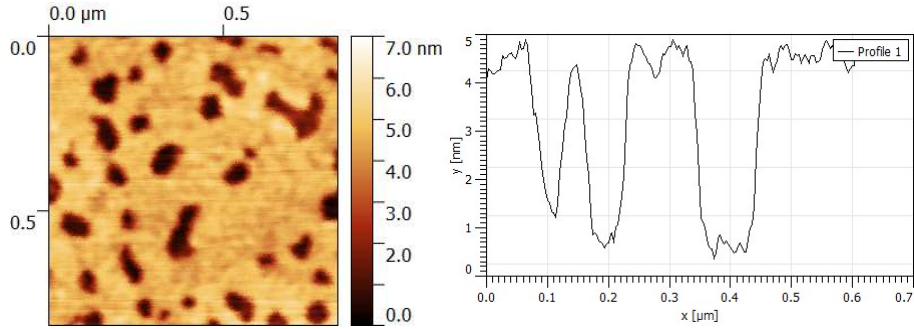**Figure S72.** AFM micrograph from the central region of a thin film.

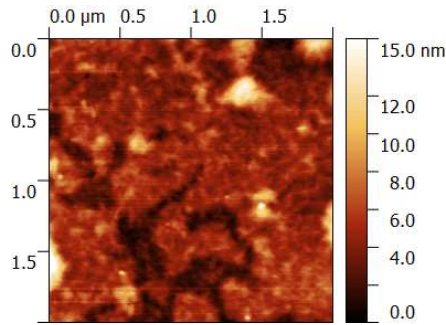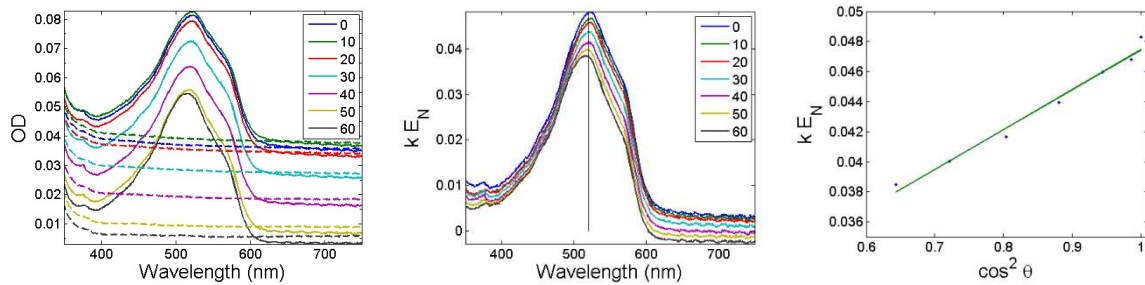Polarized Spectroscopy

Figure S73. Left) Raw data from polarized optical spectroscopy (tilt angles from 0° to 60° in steps of 10). The spin coated films are represented with solid lines and the background from the glass with dashed lines. Center) Corrected spectra given by the constant k times the absorption coefficient E_N. Right) Linear regression at the maximum of the emission to find α_{fZ}.

Trypan Blue BZK10 Hold 7

Optical Microscopy
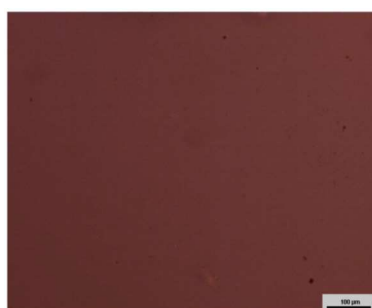
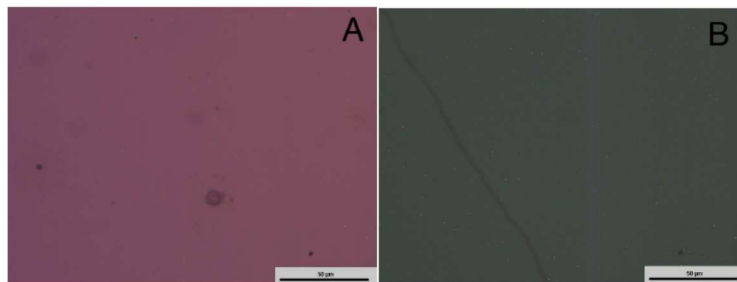**Figure S74**. Wide field optical microscopy image of the central region of a thin film.
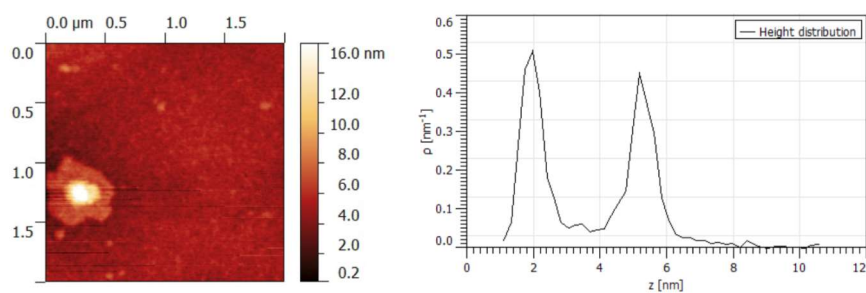
Atomic Force Microscopy
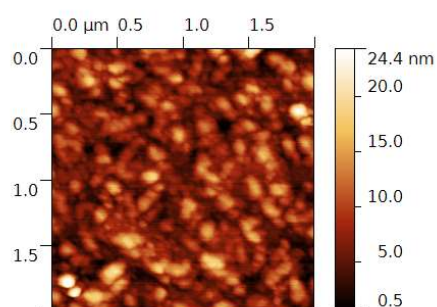
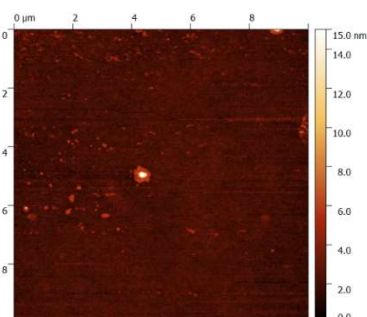**Figure S75.** AFM micrograph from the central region of a thin film.
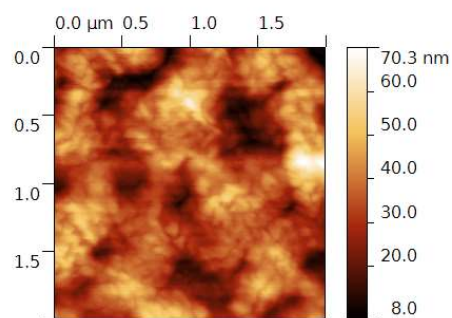
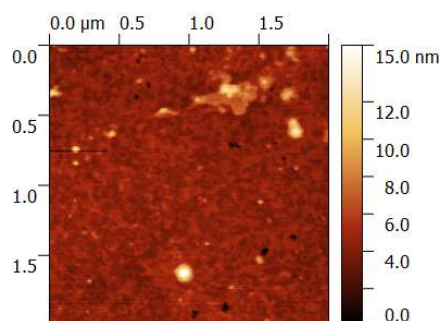**Figure S76.** AFM micrograph from the central region of a thin film.
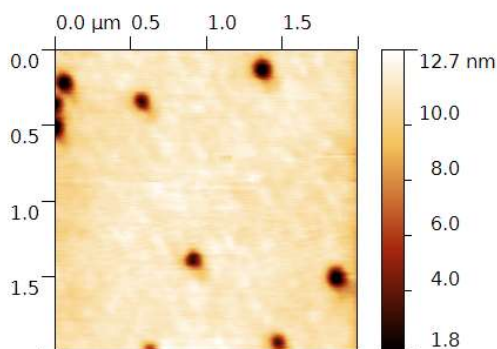
Figure S77. AFM micrograph from the central region of a thin film.

Polarized Spectroscopy
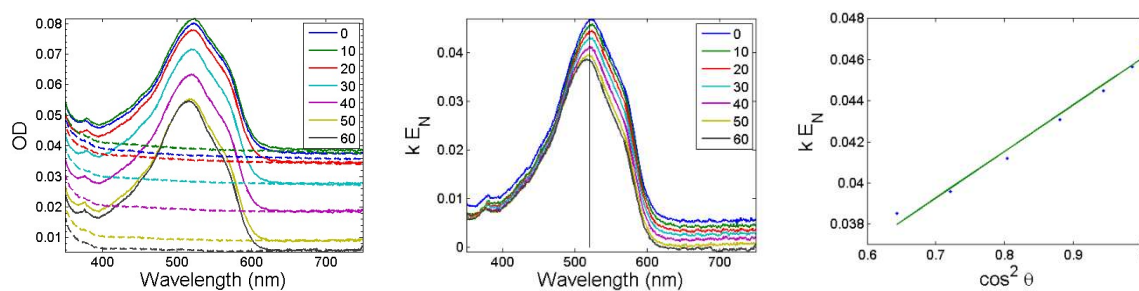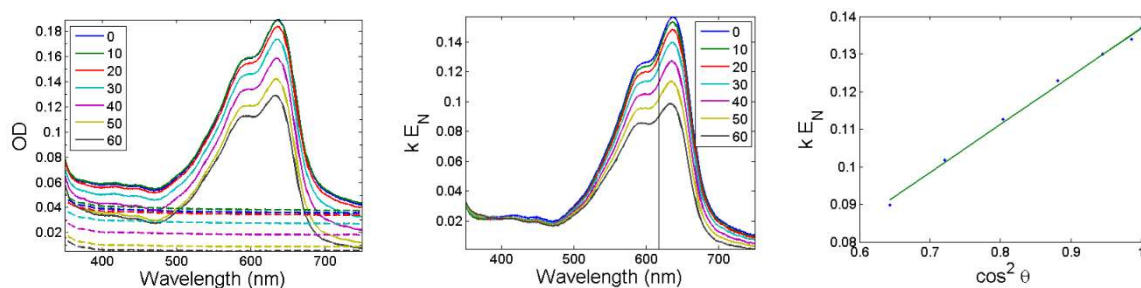

Figure S78. Left) Raw data from polarized optical spectroscopy (tilt angles from 0° to 60° in steps of 10). The spin coated films are represented with solid lines and the background from the glass with dashed lines. Center) Corrected spectra given by the constant k times the absorption coefficient E_N. Right) Linear regression at the maximum of the emission to find α_{fz}.

Polarised Spectroscopy Analysis

Figure 4 in the main text shows the data and the result from the modelling of the experimental data for Allura Red in stretched polymers. Here, the α_{fZ} angle is well defined at 48°, while the ϕ_{fz} angle can vary from ≈30° to ≈60° at the emission maximum, depending on the assumptions made regarding the overall shape of the dye molecule. The assumptions regarding the molecular shape correspond to assuming that the molecules at perfect alignment can be located at a specific point of the orientation triangle. The relation between ϕ_{fz}, the assumed shape of the molecule, and the orientation factor is plotted in Figure 4 in the main text and in Figure S79 below, using equation 5. If the molecule is considered to be rod-like it will follow the top line of the orientation triangle, while a flat-like molecule will be at the bottom edge of the orientation triangle. The numerical analysis allows us to determine the possible values ϕ_{fz} can take as a function of the position in the orientation triangle.

To analyse the data an assumption of the degree of alignment must be made. With intermediate limiting alignment (region R2) the angle between the transition moment and the stretch direction must be within the range $28° \leq \phi_{fz} \leq 68°$. If the limiting alignment with the stretch direction is better (R1) we can predict that the angle must be in the region $43° \leq \phi_{fz} \leq 53$, and if the molecule can be perfectly aligned we can determine that ϕ_{fz} will be 48°. These considerations are compiled in Table S1 for all four dyes, while figure S79 shows the orientation triangles and corresponding ϕ_{fz} vales for Allura Red and Trypan Blue. Note that the gray areas in figure S79 are excluded due to the experimentally determined values of k_f.

For the purpose of describing the direction of the transition moment in the molecular structure the data is not perfect. For the box-like molecules Allura Red, Bordeaux Red, and Amaranth we can estimate a ≈ 10° range where ϕ_{fz} must lie within when we assume an alignment of $0.7 \leq kz \leq 1$ (region R1, Figure S79). For the rod-shaped Trypan Blue a higher spread of 33° is found for that range of kz. A much narrower 4 degree range is found if we assume a higher degree of alignment $0.9 \leq kz \leq 1$ (region R1, Figure S79) than for the other molecules, due to the well-defined shape of the molecule. For the purpose of determining the molecular structure of thin films these results clearly show the orientation of the transition moments (M_f) with respect to the molecular long axis (z). The detailed data is compiled in Table S1.

Trypan Blue provides a clear example. In stretched PVA the rod-like molecule is oriented with z and Z close to the same axis i.e. k_z is close to 1. In the thin films, the Z axis is perpendicular to the lamellar, such that Trypan Blue is oriented with the long axis (z) roughly perpendicular to Z. The data shows that $\alpha_{fZ,\text{PVA}} = 33°$ while $\alpha_{fZ,\text{thin film}} = 80°$, which assuming ideal alignment $\omega_{zZ,\text{PVA}} \approx 0° \phi_{fz}$,PVA ≈ 33° corresponds to $\omega_{zZ,\text{thin film}}$ at either ≈53° or ≈113°. From a fundamental standpoint a large different, but as can be seen in Figure 4, the molecular structure in the two materials that would give rise to the different angles is small. As for Trypan Blue ϕ_{fz} ,PVA =33° is the maximum ϕ_{fz} ,PVA angle, when considering $\omega_{zZ,\text{PVA}} \neq 0°$ we can provide the boundary $53° \leq \omega_{zZ,\text{thin}} \leq 113°$.
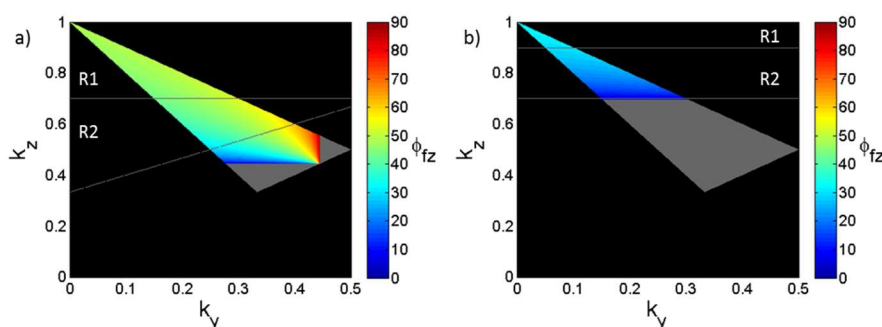

Figure S79. Orientation triangles for Allura Red (left) and Trypan Blue (right) showing the relation between ϕ_{fz} and the orientation factors is. ϕ_{fz} angle (color) satisfies the requirement $k_z \geq k_f \geq k_y$ from

Equation 5. The area of orientation triangle shaded gray is excluded by the experimentally determined value of k_f.

Table S1. Summary of the results from the numerical analysis of polarized spectroscopy data obtained on azo-dyes in stretched PVA. The results are presented as a function of the orientation factor (k_z) and the assumed shape of the molecular structure. The insert show the orientation of the transition moment (M_f) in the molecular structure of Allura Red, Bordeaux Red, Amaranth, and Trypan Blue in the case of perfect alignment ($\alpha_{fZ} = \phi_{fz}$) represented with black arrows. And in case of intermediate alignment assuming that the molecular shape is rod-like (blue arrows) or flat (red arrows).

	Allowed orientation factor range	Alura Red $\phi_{fz,max}$	Bordeux Red $\phi_{fz,max}$	Amarant $\phi_{fz,max}$	Trypan Blue $\phi_{fz,max}$
λ		514 nm	530 nm	534 nm	617 nm
Experimental k_f[a]		0.4441	0.4291	0.4593	0.6966
Perfect alignment $\alpha_{fZ} = \phi_{fz}$	$k_z = 1$	48	49	47	33
Assuming intermediate alignment	$k_z > 0.7$	43–53	45–55	41–51	29–33[b]
Possible orientation angles	$0.5/0.6 > k_z > 1$[c]	28–62	32–68	24–57	4–33[b]

[a] The number of decimals indicated does not represent the accuracy of calculating k_f, however it is important to take all the decimals in order to calculate the angles consistently. Note that the angles are not presented with such a high accuracy. [b] The experimental k_z is 0.6966 for trypan blue, the interval reported are for $k_z > 0.9$ and $k_z > 0.7$. [c] The region excluded by the experimental values of k_f is asymmetric in kz. The interval is selected from kz = 0.5 in the rod-like limit and kz = 0.6 in the flat-like limit.
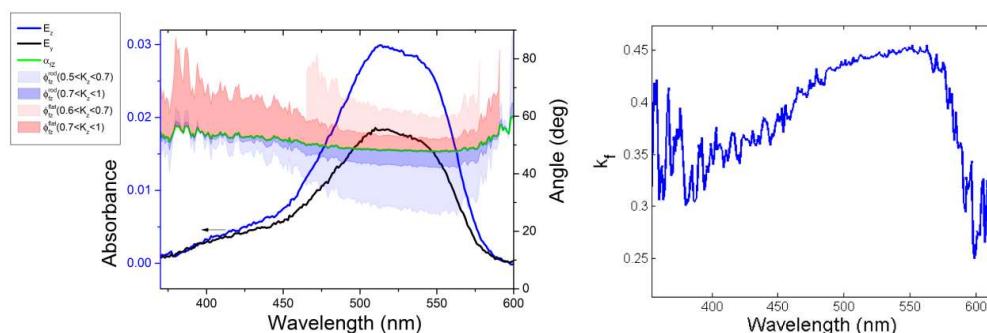
Stretched polymer analysis

Figure S80. Left: Angles respect the stretching direction of Alura Red in polyvinyl alcohol. Right: Orientation factor k_f of the transition $\boldsymbol{M}_f$ respect to the stretching direction Z.
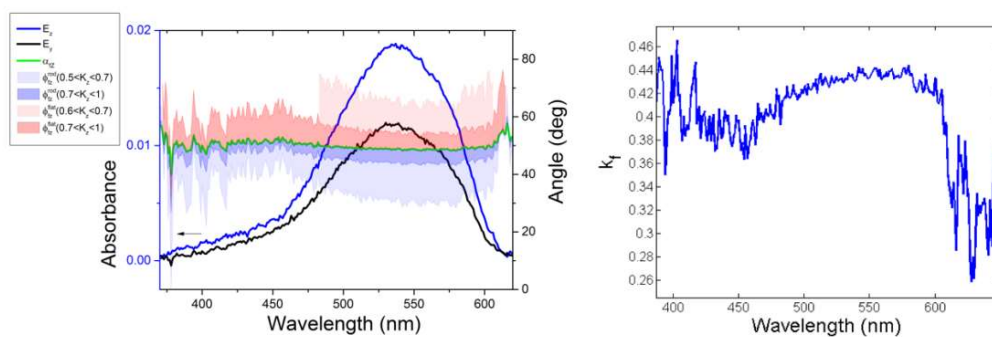

Figure S81. Left: Angles respect the stretching direction of Bordeaux Red in polyvinyl alcohol. Right: Orientation factor k_f of the transition $\boldsymbol{M}_f$ respect to the stretching direction Z.
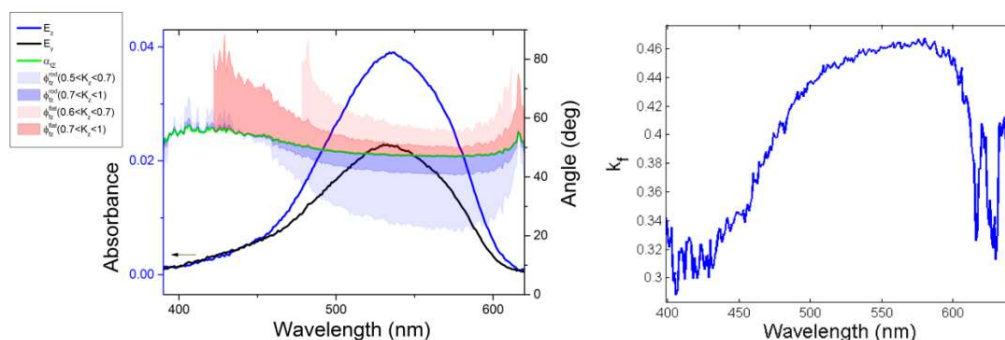

Figure S82. Left: Angles respect the stretching direction of Amarant in polyvinyl alcohol. Right: Orientation factor k_f of the transition $\boldsymbol{M}_f$ respect to the stretching direction Z.
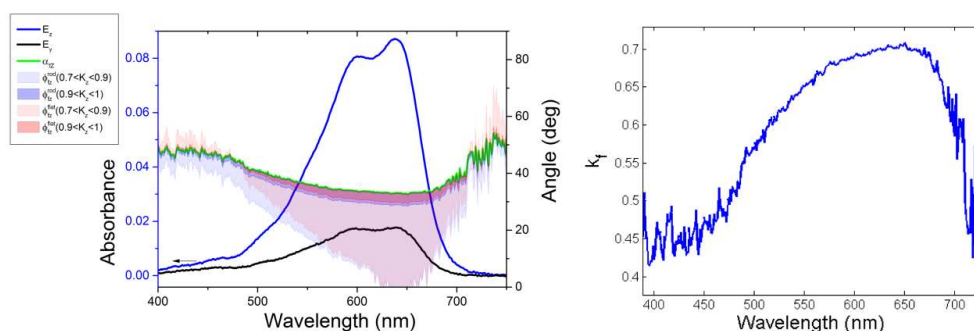
Figure S83. Left: Angles respect the stretching direction of Trypan Blue in polyvinyl alcohol. Right: Orientation factor k_f of the transition M_f respect to the stretching direction Z.
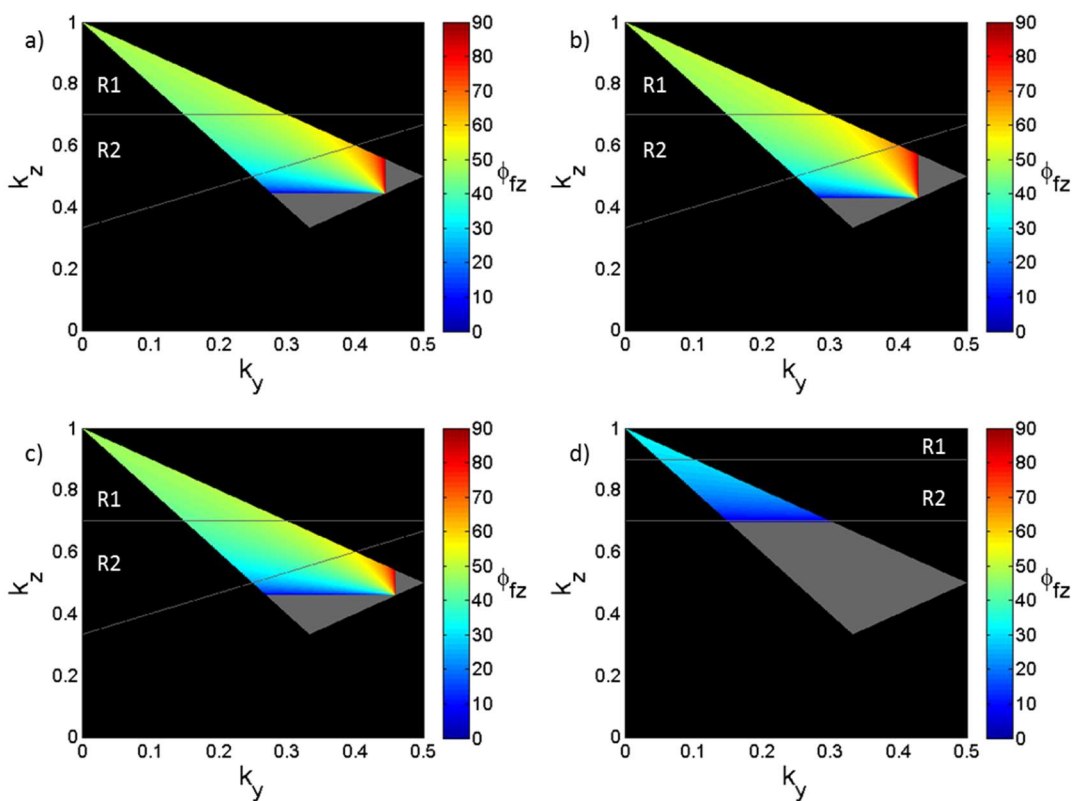

Figure S84. (**a**) Allura Red; (**b**) Bordeaux Red; (**c**) Amarant; (**d**) Tryphan Blue.
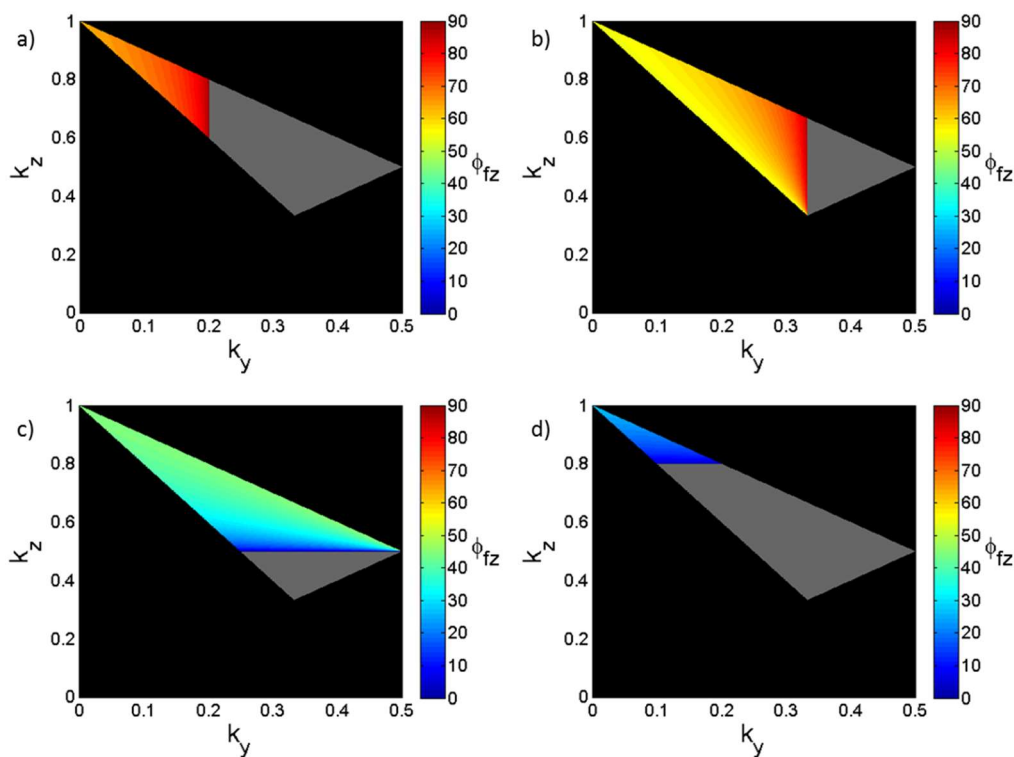

Figure S85. a) k_f=0.2 b) k_f=1/3 c) k_f=0.5 d) k_f=0.8.

Table S2. Angle between transition dipole and long molecule axes assuming planar molecules and/or rod-like orientation.

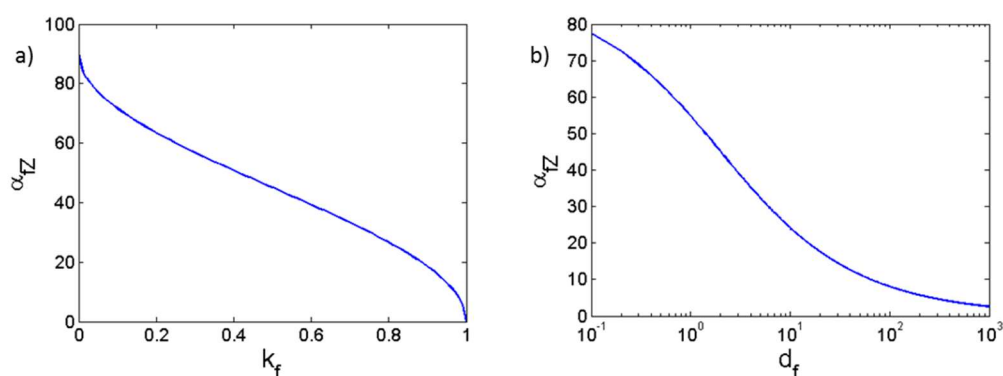| k_f	$\phi_{fz\text{min}} \leq \phi_{fz} \leq \phi_{fz\text{max}}$ (all posible values in the orientation triangle)
0.2	$63.4° \leq \phi_{fz} \leq 90°$
0.3333	$54.7° \leq \phi_{fz} \leq 90°$
0.5	$0° \leq \phi_{fz} \leq 45°$
0.8	$0° \leq \phi_{fz} \leq 26.6°$
0.4441 (Allura Red)	$0° \leq \phi_{fz} \leq 90°$
0.4291 (Bordeaux Red)	$0° \leq \phi_{fz} \leq 90°$
0.4593 (Amarant)	$0° \leq \phi_{fz} \leq 90°$
0.6966 (Tryphan Blue)	$0° \leq \phi_{fz} \leq 33°$

Figure S86. (**a**) Transition dipole angle respect to the uniaxial axes Z against k_f; (**b**) Transition dipole angle respect to the uniaxial axes Z against the dichroic ratio d_f.